Chirality

WILEY

Chirality

RESEARCH ARTICLE OPEN ACCESS

Exploring Naproxen Cocrystals Through Solid-State Vibrational Circular Dichroism

Adam Sklenář[1,2] | Anne Zehnacker-Rentien[3] | Jakub Kaminský[1] | Jan Rohlíček[4] | Petr Bouř[1,2]

[1]Institute of Organic Chemistry and Biochemistry, Academy of Sciences, Prague, Czech Republic | [2]Department of Analytical Chemistry, University of Chemistry and Technology, Prague 6, Czech Republic | [3]Institut des Sciences Moléculaires d'Orsay, CNRS, Université Paris-Saclay, Orsay, France | [4]Institute of Physics, Academy of Sciences, Prague, Czech Republic

Correspondence: Petr Bouř (bour@uochb.cas.cz)

Received: 12 December 2024 | **Revised:** 5 February 2025 | **Accepted:** 6 February 2025

Funding: This work was supported by the Czech Science Foundation (24-10558S), Ministry of Education, Youth and Sports of the Czech Republic (e-INFRA CZ 90254), University of Chemistry and Technology (A2_FCHI_2024_028), and the French National Research Agency (ANR) Dichrosol project (Grant ANR-23-CE29-0006).

Keywords: vibrational circular dichroism | solid state | density functional theory | cocrystals | naproxen | alanine | proline | spectra modeling

ABSTRACT

Vibrational circular dichroism (VCD) spectroscopy appears as a useful method for characterizing optically active substances in the solid state. This is particularly important for active pharmaceutical ingredients. However, measurement and interpretation of the spectra bring about many difficulties. To assess the experimental and computational methodologies, we explore an anti-inflammatory drug, naproxen. Infrared (IR) and VCD spectra of the pure compound and its cocrystals with alanine and proline were recorded, and the data were interpreted by quantum chemical simulations based on a cluster model and density functional theory. Although unpolarized IR spectroscopy can already distinguish pure ingredients from cocrystals or a mixture, the VCD technique is much more sensitive. For example, the naproxen carboxyl group strongly interacts with the zwitterionic alanine in the cocrystal via two strong hydrogen bonds, which results in a rather rigid structure crystallizing in the chiral $P2_12_12_1$ Sohncke group and its VCD is relatively strong. In contrast, the D-proline and (*S*)-naproxen cocrystal ($P2_1$ group) involves a single hydrogen bond between the subunits, which together with a limited motion of the proline ring gives a weaker signal. Solid-state VCD spectroscopy thus appears useful for exploring composite crystal structures and interactions within them, including studies of pharmaceutical compounds.

1 | Introduction

Solid state is a very convenient form of drug delivery [1]. It can circumvent the low solubility of active pharmaceutical ingredients (API) and improve their bioavailability or stability [2]. For example, from Class II of the Biopharmaceutics classification system containing low-solubility drugs, 30% of all marketed products are in the solid state [3]. Structural characterization of such compounds is essential to ensure their proper activity, safety, and regulatory approval.

For the crystal structure determination, diffraction methods including powder diffraction remain the gold standard [4, 5]. Solid-state nuclear magnetic resonance (NMR) spectroscopy does not provide atomic resolution, but offers insight into the chemical composition and molecular packing as well [6]. The construction of the crystal structure from such data is sometimes referred to as NMR crystallography [7]. One can also use cryo-electron [8] or transmission electron microscopies [9].

Compared to these techniques, infrared absorption (IR) and vibrational circular dichroism (VCD) offer a relatively simple, fast, and inexpensive experiment, still sometimes surprisingly sensitive to the structure and composition. The (in principle) non-destructive nature of IR techniques enables the treatment of expensive samples, or of these available in small quantities.

Unlike for spectroscopies using visible light, almost all compounds provide absorption bands useful for solid-state IR studies [10–12]. The chiral extension of IR, VCD, is in addition sensitive to chirality, detecting differential absorption of the left and right circularly polarized light [13]. Since more than 50% of all drugs are optically active, this technique can be used for a large segment of APIs [14].

In general, VCD is also more sensitive to the structure than IR [15, 16]. The price to pay is the weakness of the differential signal. The typical ratio of VCD to IR is about 10^{-4}, which makes the experiment prone to artifacts. Solid-state VCD (ssVCD) experimental procedures thus involve additional steps minimizing the false signals in the spectra. For example, it is very convenient when both enantiomers of investigated systems are available for the measurement [17]. It has been shown that ssVCD can distinguish crystal polymorphs [18], hydrates from dried API [19], different solvates [20] or pure compound from a cocrystal [17, 21].

For interpretation of ssVCD spectra, methods fully exploring the crystal periodicity are often based on first principle molecular dynamics simulations and the nuclear velocity perturbation theory in a plane waves approach [22–24]. These are often restricted to general gradient approximation functionals [25]. A much simpler way consists of extracting a cluster of limited size from the crystal structure and calculating its spectroscopic properties. However, this approach does not fully take into account the environmental effects in the whole crystal [26, 27]. Even when the periodic boundary conditions are used for the optimization of a subunit, edge effects appear in the spectra and complicate their interpretation. In this work, we use an extended cluster approach that allows us to treat bigger systems using more precise (hybrid) functionals in the frame of the magnetic field perturbation theory [28, 29]. Vibrational properties are calculated for smaller parts of the crystal and transferred back using the Cartesian coordinate tensor transfer (CCT) technique [30, 31]. In particular, the Hessian (force constant matrix) and the phonon modes can be obtained in this way.

The CCT-based approach appeared extremely flexible and was previously applied to systems of thousands of atoms [32], crystal assemblies [17, 33], or liquids [29]. For crystal, the periodicity is fully considered by calculating the dynamic force field matrix of the elementary cell for the zero-phonon mode determining the optical spectra. Longer-range forces could in principle be included in the model, for example, by adding larger fragments calculated at a lower approximation level. Compared with ad hoc cluster approaches [20, 21, 34, 35], the fragmentation is automatized and flexible, based on pre-defined interaction distances and desired cluster sizes. Although probably not suitable for crystals with long-range electron conjugation, this computational methodology provided a basic understanding of the spectral features and a solid basis for spectral band assignment for the molecular systems studied here.

Cocrystals are convenient systems to explore how the VCD methodology captures various structural differences. They can be universally found in the realm of APIs. A cocrystal is a crystalline material composed of two or more compounds within a single crystal lattice. In what follows, we focus on the cocrystal of the anti-inflammatory drug naproxen with alanine and proline as a cocrystal formers (coformers) (Figure 1). We investigate whether ssVCD is able to distinguish the cocrystals from a pure APIs and a mixture of pure solid components.

2 | Methods

2.1 | Sample Preparation

Commercially available (*R*) and (*S*)-naproxen (Merck, pharmaceutical impurity standard) and L or D-alanine/proline (Fluka) were used without further purification. The cocrystals were prepared using a liquid-assisted grinding (LAG) method, consisting of grinding the solid components with a small amount of solvent [36] following refs. [37] and [38]. Cocrystals of (*S*)-naproxen and L-alanine (and enantiomeric form), (*S*)-naproxen and D-alanine, (*S*)-naproxen and D-proline (and enantiomers), and (*S*)-naproxen and L-proline were prepared. To explore the computational analysis, the (*S*)-naproxen/L-alanine and (*S*)-naproxen/D-proline combinations were analyzed in detail. The chemicals were ground together at ambient conditions for 60 min at a 1:1 stoichiometric ratio with 10 μL of methanol added to 100 mg of the mixture. We found that the cocrystal formation does not depend strongly on the amount of methanol. For a test measurement, partially cocrystallized sample of (S)-naproxen and L-alanine (in 1:1 mass ratio, i.e., with molar excess of alanine) and its enantiomer were prepared as well, which gave spectra close to a sum of the cocrystal and excessive alanine (Figure S1). Retsch Mixer Mill MM 200 with three stainless steel balls of 0.5 cm diameter was used. Finally, pellets were made by mixing the analyte with the KBr matrix in a ratio of about 1:100, adjusted to optimize the maximal absorbance within 0.8–1.0, and pressing.

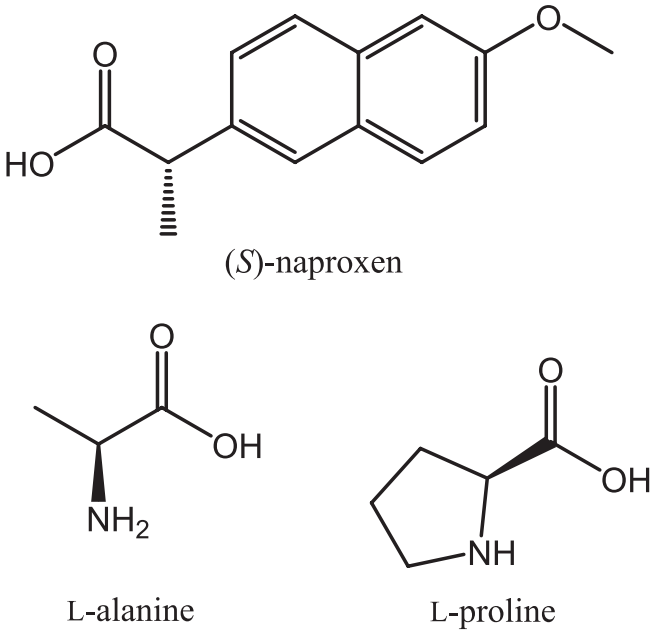

FIGURE 1 | Studied compounds.

2.2 | Measurement of Vibrational Spectra

IR and VCD spectra were recorded using two spectrometers, according to availability or for a verification: a ChiralIR-2XTM spectrometer (BioTools, Inc., USA) equipped with a dual-PEM™ system using two ZnSe photoelastic modulators and a Bruker Vertex70 spectrometer with VCD extension (PMA 50 Bruker), consisting of a photoelastic modulator (PEM) and a fast-acquisition dual channel. A previously described procedure was used to minimize instrumental artifacts, which is documented in ref. [17] and its rich supporting material. As reported in the literature, most artifacts can be eliminated by averaging the orientations of the sample (flipping) combined with its continuous rotation around the beam axis [39, 40]. In our case, we found that the effect of flipping was rather minor [17]. Control measurements were conducted for a suspension in nujol oil. A 4 cm^{-1} resolution, the Blackman–Harris apodization function, and PEM calibration at 1400 cm^{-1} were used. The resulting spectra are averages of six recorded blocks, with each one consisting of 1560 scans. The experiment took approximately 3 h for each sample.

2.3 | X-Ray Powder Diffraction

At the Université Paris-Saclay, powder X-ray diffraction (PXRD) patterns were recorded at the MORPHEUS platform of the Laboratoire de Physique des Solides at room temperature on a Bruker D8 Advance diffractometer equipped with a LYNXEYE position-sensitive detector, using Cu Kα radiation ($\lambda = 0.15418$ nm). Other experiments were performed at the Institute of Physics of Prague, where the sample was ground and placed in a 0.5-mm borosilicate-glass capillary. Powder diffraction data were collected using the Debye–Scherrer transmission configuration on a powder diffractometer Empyrean (PANalytical, $\lambda_{Cu,K\alpha} = 0.15418$ nm), equipped with a focusing mirror, capillary holder, and a PIXcel^{3D} detector. The measurement range was 3–80° 2θ with a 0.013° step size and 150 s per step.

2.4 | Modeling and Calculations

Fragmentation and tensor transfer approaches [17, 30, 31] were used, where the basic crystal model consisted of 27 elementary cells. It was obtained by propagating the elementary cell three times in each crystallographic direction (*a*, *b*, *c*). X-ray geometries downloaded from the Cambridge Crystallographic Data Centre (CCDC) were used for alanine, proline, naproxen, and the cocrystals (Table S1). Using our scripts [29], smaller fragments were created comprising interactions of all molecules in the central elementary cell with the closest ones. The fragment geometries were partially optimized in the vibrational normal mode coordinates [41, 42], and harmonic force constants, atomic polar, and axial tensors were calculated at the B3LYP [43]/6–311++G** [44] level comprising the GD3BJ [45] dispersion correction. The Gaussian 16 Rev.A.03 program package [46] was used for the quantum chemistry calculations.

Similarly, as in previous studies [35, 47], we used the CPCM [48](H_2O) solvent model to mimic the crystal environment, in particular the effect of the polar groups. Note that within the CPCM methodology, the main parameter is the dielectric constant and the result are not particularly sensitive to it for large relative permittivities. For our systems, the CPCM environment is particularly important as it also stabilizes zwitterionic forms of the amino acids.

The vibrational parameters were transferred back to the 27-cell system, and the force constants matrix and zero-phonon spectra calculated [49]. For the naproxen/proline cocrystal where the x-ray data [50] indicated two geometries of the proline ring, the spectra were simulated for both possibilities and averaged (cf. Table S2; Figure S2). In addition, the effect of longer-range interactions was explored using the transition dipole coupling model [51, 52]. From the dipole and rotational strengths, IR and VCD spectra were generated by convolution with a Lorentzian function, using full width at half height of 10 cm^{-1}.

3 | Results and Discussion

3.1 | Crystal and Cocrystal Structure

X-ray geometries of naproxen and its cocrystals with alanine and proline (CCDC identifiers COYRUD, RODSEK and FEVZOX, respectively) are displayed in Figure 2. Clearly, the packing patterns

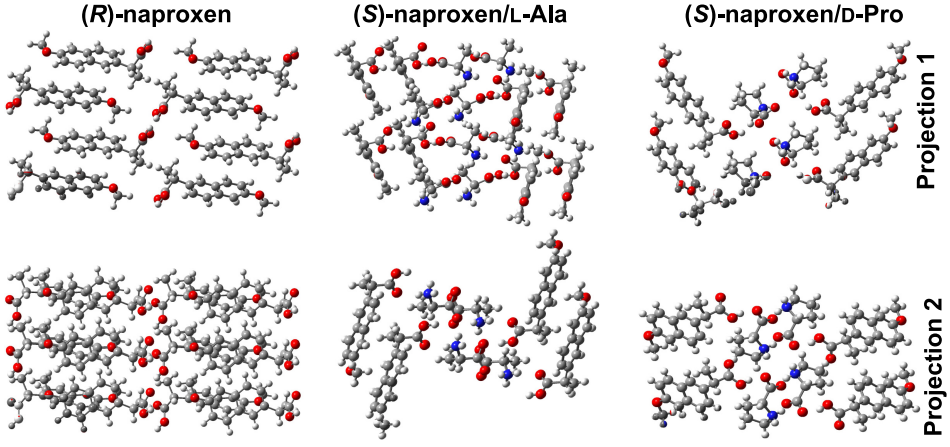

FIGURE 2 | Crystal packing in naproxen and the two cocrystals, in two projections.

are different. In pure naproxen ($P2_1$ symmetry), the carboxyl groups are linked by H-bonds and the naphthyl subunits are in a parallel-displaced geometry, allowing for a limited π–π interaction. In both cocrystals, the amino acids are present as zwitterions, and the naproxen molecules are not directly connected by H-bonds. In the naproxen/alanine system ($P2_12_12_1$ Sohncke symmetry group), the NH_3^+ residue is bonded to the O=C group of naproxen, and the aromatic rings adopt parallel-displaced positions, allowing for a more favorable overlap between the π clouds than in pure naproxen. For naproxen/proline ($P2_1$ Sohncke symmetry group), the proline NH_2^+ group is H-bonded to other prolines only, whereas the naproxen interacts with the carboxylate group of the amino acid. The naproxen–naproxen packing seems to be looser here, with the naphthyl planes tilted more to each other than in the naproxen/alanine cocrystal.

3.2 | Powder Diffraction

The formation of the cocrystals was confirmed by powder X-ray diffraction (PXRD) measurements. The observed diffraction patterns were compared with those calculated from previous studies [38], providing evidence of the cocrystal formation (Figure 3). The patterns are almost identical, although in the naproxen/alanine cocrystal data additional weak peaks indicate a small contamination of the sample by crystalline alanine. Such impurities may have resulted from the different solubilities of naproxen and alanine in methanol. The data analyzed below, however, do not indicate that the impurities have a detectable influence on the vibrational spectra.

3.3 | Solid-State Vibrational Circular Dichroism Experiments

IR and VCD spectra of the pure components, naproxen, alanine, and proline, are plotted in Figure 4. The "mirror imaging" of the S/R and D/L enantiomers confirms reliability of the experimental protocol [17]. Most visible distortions of naproxen VCD spectra appear in the regions around 1200 cm^{-1} and 900 cm^{-1}. Alanine and proline give straighter VCD baseline and fewer artifacts. Overall, VCD signal of a reasonable quality is recorded, comparable with previous studies [17, 21, 25, 53].

IR absorption and VCD spectra of (*S*)-naproxen/l-Ala and (*S*)-naproxen/D-Pro cocrystals are plotted in Figure 5, and the band assignment is given in Table 1. Experimental noise is indicated by gray lines. Clearly, the two cocrystals give different IR and VCD spectra, and the spectra differ from those of individual components. In the naproxen/alanine system (left in the figure), for example, the carbonyl bands converge and overlap. Band 4, corresponding to the symmetric bending (umbrella) vibration of the NH_3 group, is blue-shifted by 4 cm^{-1} relative to the bare L-alanine and changes VCD sign. The strong signals (13) come from the naphthyl ring, the solitary bands 14 and 15 correspond

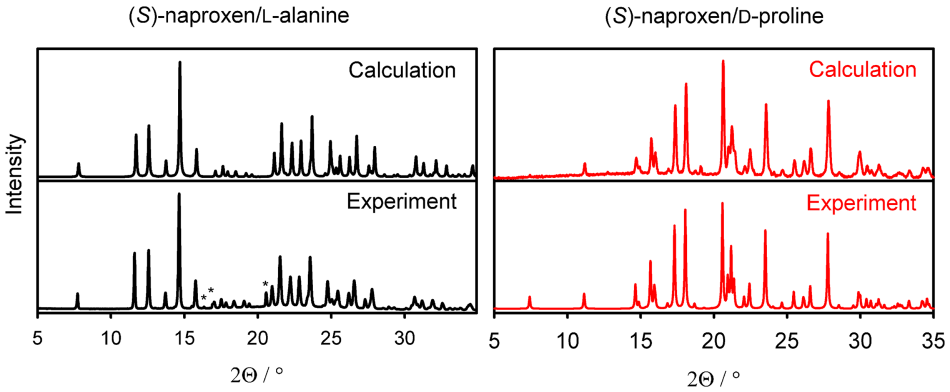

FIGURE 3 | Experimental PXRD intensities of polycrystalline LAG S-naproxen/L-alanine, peaks due to contamination with crystalline alanine marked by asterisks (*), and (S)-naproxen/D-proline cocrystals, and calculated patterns based on the crystal structure [38].

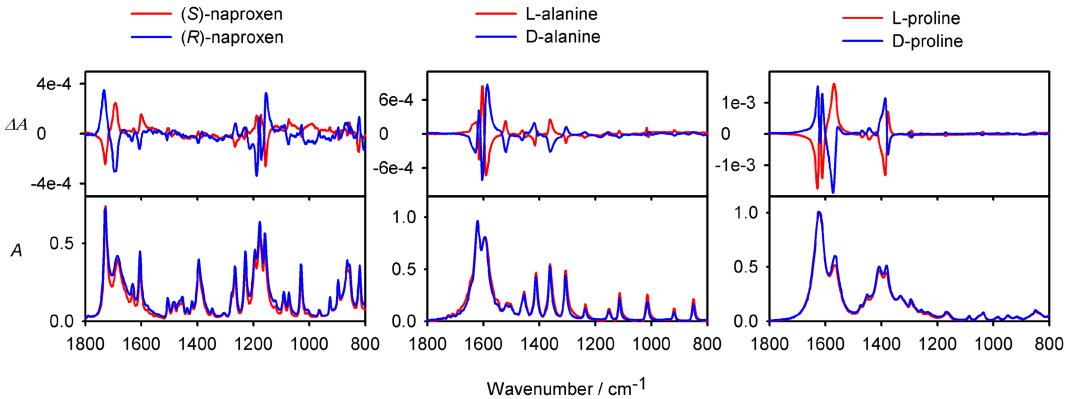

FIGURE 4 | Experimental VCD (ΔA) and IR (A) spectra of naproxen, alanine, and proline enantiomers.

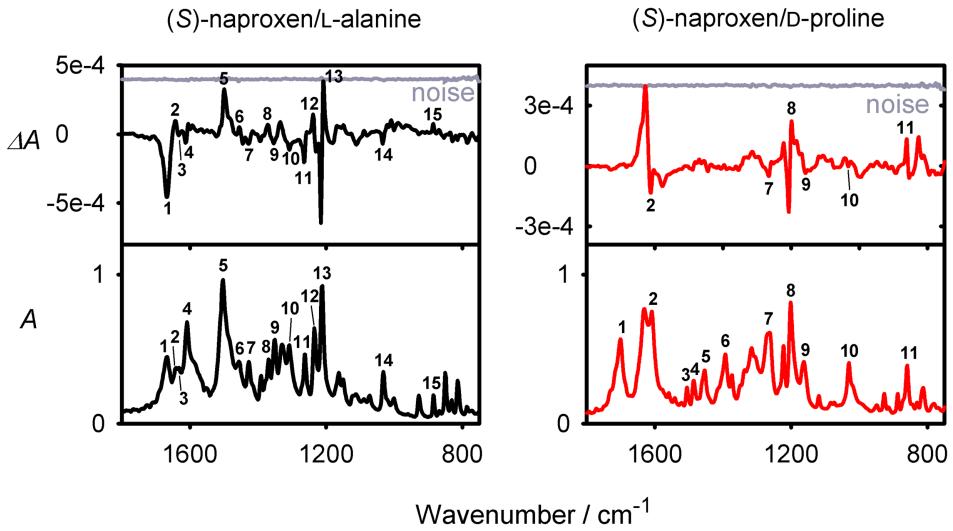

FIGURE 5 | Experimental VCD and absorption spectra of the (*S*)-naproxen/L-Ala and (*S*)-naproxen/D-Pro cocrystals, cf. Table 1 for the band assignment. The gray lines represent the experimental noise.

to out of plane vibrations of the carboxylate group and C-C bond stretching in naproxen. Band 1 of the C=O stretching of naproxen appears as a strong negative peak in the VCD spectrum at 1667 cm^{-1}. The strong difference compared to pure naproxen probably arises from the different nature of the hydrogen bond, neutral OH ... O in naproxen vs. ionic NH^+ ... O in the cocrystal. Indeed, in the naproxen/proline cocrystal where this type of H-bonding does not exist the C=O naproxen stretching frequency is observed much higher, at 1710 cm^{-1}.

VCD intensities of the naproxen/alanine are on average stronger than those of the naproxen/proline cocrystal (Figure 5, right). In addition, the IR absorption is much broader for the latter. Several hypotheses could explain these differences: first, the two cocrystals crystallize in different space groups ($P2_1$ for proline and $P2_12_12_1$ for alanine), which can affect the VCD intensity [54]. For example, non-local effects enabled by the crystal packing can enhance it [55, 56]. Second, the conformational mobility of proline is larger than that of alanine, as both puckering isomers can exist in the crystal. This might result in a blurring of the VCD spectrum due to the contribution of the two isomers. For naproxen/alanine the interaction between the two components involves two strong ionic hydrogen bonds, which makes the system more conformationally stable and rigid than for naproxen/proline involving one hydrogen bond only.

These VCD and IR spectra are compared with those of the complementary combinations, (*S*)-naproxen/D-Ala and (*S*)-naproxen/L-Pro, in Figure S3, part a. One can see that while IR spectra of the diastereoisomers are rather similar, VCD spectra exhibit profound differences. "Mirror images" of VCD for enantiomers of (*S*)-naproxen/L-Pro and (*S*)-naproxen/D-Pro in Figure S3b reveal an artifact for (*S*)-naproxen/L-Pro around 1735 cm^{-1}; otherwise, the quality of the spectra seems reasonable given the weakness of the signal in these cases.

The cocrystal IR and VCD spectra are also different from those obtained as mere sums of the two components. For naproxen/alanine, this is shown in Figure 6, where we see that whereas the spectra of a 1:1 M ratio mixture can be obtained as the sum, the cocrystal behaves as an autonomous species.

3.4 | Spectra Simulations

To explore the variations coming from parameters used in the fragmentation methodology, we simulated IR and VCD spectra of alanine. Second energy derivatives, atomic polar and axial tensors were calculated including molecular pairs, trimers, and a cluster of one molecule with 14 neighboring ones in the crystal ("15-mer"). After the tensors were transferred back to the crystal, the dynamic force field matrix was calculated, and resultant spectra are plotted in Figure S4. For all models, a problematic part of the spectrum is the region of 1720–1560 cm^{-1}, including N–H bending (band 1) and C=O stretching (band 2). Perhaps by accident, the trimer gives the best result here. Other calculated IR and VCD bands reproduce the experimental ones better, and their intensities are not so much dependent on the details of the fragmentation approach.

For the cocrystals, with our computational resources we were limited to the pair-wise fragmentation scheme, which gave the spectra plotted in Figure 7. Given the approximations, we consider the agreement with the naproxen/alanine experiment to be very good, providing reliable assignment for most of the strongest IR and VCD spectral features (Table 1). The frequency of the C=O stretching band (#1) is calculated too high, but with reasonable intensities and correct VCD sign. Around 1300 cm^{-1} the band assignment based on IR would be problematic; however, VCD with the sign information is quite helpful in this respect. The 1,030 cm^{-1} −/+ VCD couplet in the experiment is reproduced with a lower intensity only.

For naproxen/proline, the agreement is not so good. The computation reproduced the trends in the C=O stretching frequencies, which are significantly lower (exp./cal. 1667/1731 cm^{-1}) in naproxen/alanine than in naproxen/proline (1710/1761 cm^{-1}). This is due to the much stronger hydrogen bonding of the

TABLE 1 | Experimental and calculated vibrational frequencies (cm^{-1}) of the (*S*)-naproxen/L-alanine and (*S*)-naproxen/D-proline cocrystals.

Band[a]	$\omega_{Exp(VCD)}$	ω_{Calc}	VCD sign	Assignment
(*S*)-naproxen/L-alanine				
1	1667	1731	−	ν(C=O) naproxen
2	1642	1662	+	Asym. δ (NH_3) alanine
3	1633	1646	−	Naphthalene core naproxen, ν(C=C)
4	1612	1627	−	Sym. δ (NH_3) alanine
5	1498	1514	+	δ, C-H, CH_3 naproxen
6	1455	1462	+	δ(O-H) naproxen
7	1427	1419	−	Sym. δ (CH_3) alanine; δ(C-H), ν(C-C) naproxen
8	1372	1396	+	δ (CH_3)
9	1354	1357	−	δ, C-H, O-H naproxen
10	1307	1320	−	δ(C-H) alanine
11	1265	1291	−	δ(C-H), naphthalene ring
13	1215	1213	−	ν(C-C), δ(C-H) naproxen
13	1207	1213	+	δ (CH_3). oop (COOH) naproxen
14	1033	1028	−	Delocalized, naproxen
15	885	908	+	Naproxen methyl group def.
(*S*)-naproxen/D-proline				
1	1710	1761	+	ν(C=O) naproxen
2	1626	1634	+	Asym. ν(C=O), Pro
2	1609	1615	−	δ(N-H), Pro
3	1504	1540	+	δ(C-H), naproxen, arom.
4	1485	1515	−	δ(C-H), Pro
5	1454	1496	−	δ(C-H), naproxen, methyl scissor
6	1393	1397	−	δ(C-H), Pro, naproxen
7	1264	1246	+	ν(C-C), δ(C-H) naproxen
8	1209	1194	−	δ(C-H), naproxen, arom
8	1197	1199	+	δ(C-H), naproxen, arom
9	1164	1172	−	δ(C-H), naproxen, arom
10	1031	1038	−	ν(C-C), δ(C-H) naproxen
11	858	843	−	δ (CH_3). oop (COOH) naproxen

Abbreviations: ν, stretching; δ, bending; oop, out of plane.
[a]Figure 5.

carboxyl to the NH_3^+ group in the former. The overall absorption profile is also reasonable, given the unresolved background-like signal in the experiment.

Regarding VCD, the intensities computed for naproxen/proline (a typical VCD/absorption ratio of ~ 5×10^{-5}) are much smaller than for naproxen/alanine (~ 1.5×10^{-4}), which corresponds to the experiment. The w-shape of the aromatic naproxen signals around 1200 cm^{-1} is also reproduced correctly, whereas the calculated couplet around 1035 cm^{-1} has much lower intensity experimentally. The predicted 1634/1615 cm^{-1} "−/+" VCD band pair is seen only in nujol, whereas a positive signal was measured in the KBr pellet, indicating possible artifacts in the ssVCD measurement. For naproxen/proline, the computations predict more than four times lower intensity of the C=O stretching mode than for naproxen/alanine. This agrees with the experimental trend, although the observed signal is even weaker (cf. also Figure 5, band 1). Further weakening may occur due to a limited motion of the naproxen carboxylate groups, not included in the calculations. The dynamical factors may also explain the splitting of both C=O stretching IR bands (1 and 2), hardly discernable in the simulation. Around 1450 cm^{-1} a positive VCD is predicted, not seen in experiment; again, this can be explained by a limited motion of the five-membered proline ring in the crystal, averaging out the CH bending VCD signals, and similar anharmonic effects [57].

IR and VCD spectra simulated for the two proline ring conformations are plotted in Figure S5. Indeed, the averaging leads to partial cancelation of the VCD signal, in particular around 1300 cm^{-1}, although it cannot explain all observed features. In Figure S6, we compare the spectra of the naproxen/proline cocrystal simulated with and without the transition dipole coupling correction. While the spectra suggest that the longer-range interactions in the crystal simulated by the correction may be important for fine VCD pattern of the C=O stretching, they do not principally change the overall shape. Note also, because of the weakness of VCD, that we cannot rule out experimental artifacts for naproxen/proline, especially those competing with weak VCD signals.

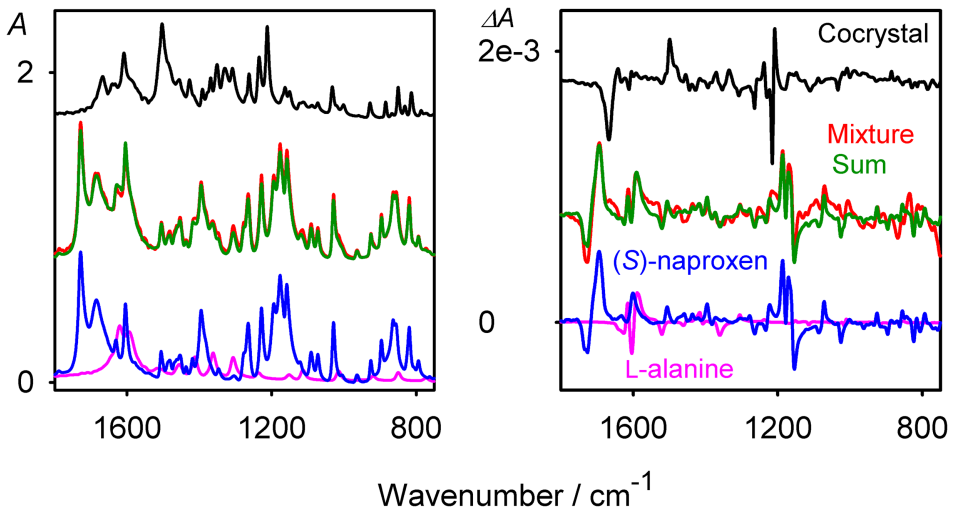

FIGURE 6 | Experimental absorption and VCD of (*S*)-naproxen/L-alanine cocrystal (black), (*S*)-naproxen/L-alanine mixture in the same 1:1 M proportion (red), sum of L-alanine and (*S*)-naproxen spectra (green), L-alanine (pink), and (*S*)-naproxen (blue).

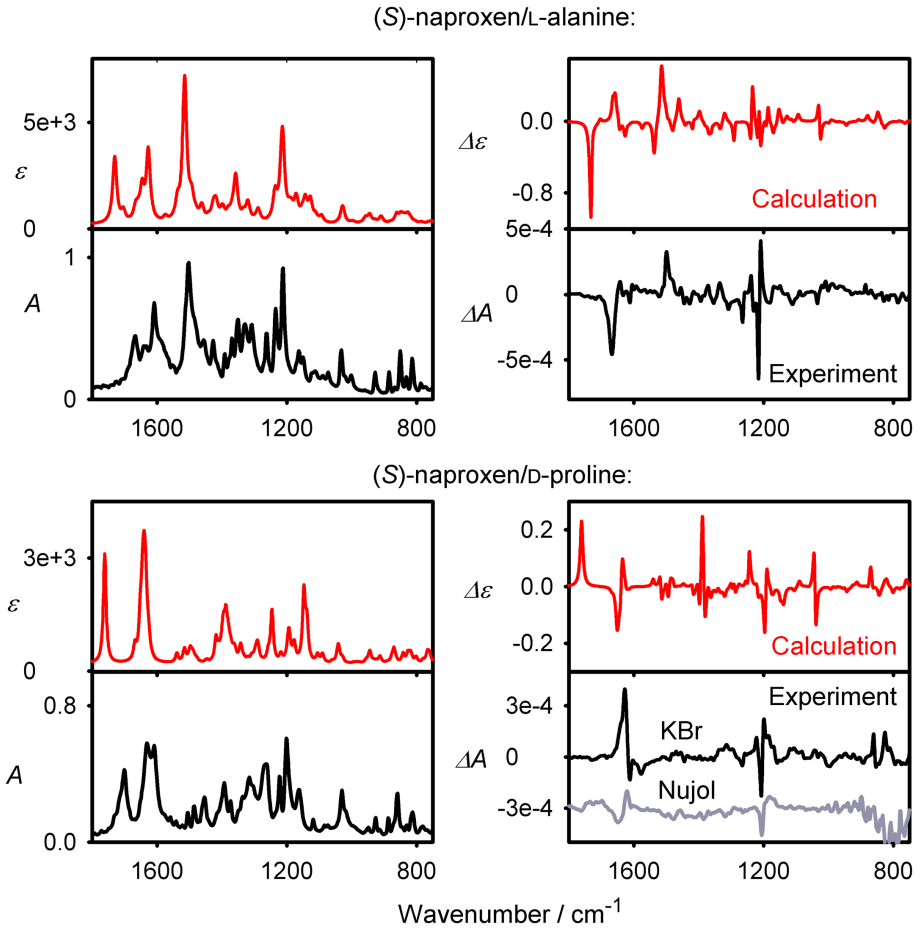

FIGURE 7 | Calculated and experimental IR absorption and VCD spectra of the (*S*)-naproxen/L-alanine and (*S*)-naproxen/D-proline cocrystals.

Overall, however, we find the IR/VCD methodology viable to study the cocrystals capturing very sensitively the structural details, such as giving clearly different spectra between mere mixtures and true cocrystals. In spite of the drawbacks, the computational methodology appears indispensable to interpret, understand, and verify the experimental solid state VCD data for the naproxen cocrystals. The advantages of combining the polarized and unpolarized spectroscopy can be documented, for example, for the region of 1200 cm^{-1} where the absorption of the naproxen/alanine cocrystal does not significantly deviate from that of the solid mixture, whereas VCD spectrum is very different.

4 | Conclusions

In our study of the naproxen–alanine and naproxen–proline cocrystals, we aimed to evaluate the solid-state vibrational circular dichroism (VCD) methodology for structural identification and confirmation. Additionally, we sought to assess the feasibility of computational approaches for interpreting the spectra. The results were promising, as the experimental protocol yielded spectra with minimal artifacts, although these were still present in the naproxen/proline cocrystal providing very weak VCD signal. In spite of that, the cocrystals could be clearly distinguished from the pure components or their mere mixtures. Due to the relatively large cocrystal size, the fragmentation computational model had to be restricted to the closest pair-wise interactions. However, it proved to be flexible and adaptable with respect to the computational sources available. For the molecular crystals studied, the model was able to reproduce the main experimental features and trends. More generally, the higher sensitivity of VCD to crystal morphology, combined with advances in experimental methods, makes this approach an interesting tool for distinguishing polymorphic forms, probing intermolecular interactions, crystal dynamics, and studying structural chirality, particularly in the pharmaceutical context.

Acknowledgments

This work was supported by the Czech Science Foundation (24-10558S), Ministry of Education, Youth and Sports of the Czech Republic (e-INFRA CZ 90254), University of Chemistry and Technology (A2_FCHI_2024_028), and the French National Research Agency (ANR) Dichrosol project (Grant ANR-23-CE29-0006). Open access publishing facilitated by Ustav organicke chemie a biochemie Akademie ved Ceske republiky, as part of the Wiley - CzechELib agreement.

Data Availability Statement

The data that support the findings of this study are available in the supplementary material of this article.

References

1. L. S. Taylor, D. E. Braun, L. Tajber, and J. W. Steed, "Crystallizing the Role of Solid-State Form in Drug Delivery," *Crystal Growth & Design* 22, no. 8 (2022): 4663–4665.

2. P. H. Karpinski, "Polymorphism of Active Pharmaceutical Ingredients," *Chemical Engineering and Technology* 29, no. 2 (2006): 233–237.

3. I. Nikolakakis and I. Partheniadis, "Self-Emulsifying Granules and Pellets: Composition and Formation Mechanisms for Instant or Controlled Release," *Pharmaceutics* 9, no. 4 (2017): 50.

4. E. S. Ameh, "A Review of Basic Crystallography and X-Ray Diffraction Applications," *Journal of Advanced Manufacturing Technology* 105, no. 7 (2019): 3289–3302.

5. Z. Huang, H. Suzuki, M. Ito, and S. Noguchi, "Direct Detection of the Crystal Form of an Active Pharmaceutical Ingredient in Tablets by X-Ray Absorption Fine Structure Spectroscopy," *International Journal of Pharmaceutics* 625 (2022): 122057.

6. P. H. Chien, K. J. Griffith, H. Liu, Z. Gan, and Y. Hu, "Recent Advances in Solid-State Nuclear Magnetic Resonance Techniques for Materials Research," *Annual Review of Materials Research* 50, no. 1 (2020): 493–520.

7. B. Elena, G. Pintacuda, N. Mifsud, and L. Emsley, "Molecular Structure Determination in Powders by NMR Crystallography From Proton Spin Diffusion," *Journal of the American Chemical Society* 128, no. 29 (2006): 9555–9560.

8. J. García-Nafría and C. G. Tate, "Cryo-Electron Microscopy: Moving Beyond X-Ray Crystal Structures for Drug Receptors and Drug Development," *Annual Review of Pharmacology and Toxicology* 60, no. 1 (2020): 51–71.

9. D. Zhang, Y. Zhu, L. Liu, et al., "Atomic-Resolution Transmission Electron Microscopy of Electron Beam–Sensitive Crystalline Materials," *Science* 359, no. 6376 (2018): 675–679.

10. D. E. Bugay, "Characterization of the Solid-State: Spectroscopic Techniques," *Advanced Drug Delivery Reviews* 48, no. 1 (2001): 43–65.

11. A. Erxleben, "Application of Vibrational Spectroscopy to Study Solid-State Transformations of Pharmaceuticals," *Current Pharmaceutical Design* 22, no. 32 (2016): 4883–4911.

12. C. Strachan, J. Saarinen, T. Lipiäinen, et al., "Spectroscopic Methods in Solid-State Characterization," in *Characterization of Pharmaceutical Nano and Microsystems*, eds. L. Peltonen, D. Douroumis, A. Fahr, J. Siepmann, M. J. Snowden, and V. P. Torchilin (Weinheim: Wiley, 2021): 27–95.

13. T. A. Keiderling, "Structure of Condensed Phase Peptides: Insights From Vibrational Circular Dichroism and Raman Optical Activity Techniques," *Chemical Reviews* 120, no. 7 (2020): 3381–3419.

14. L. A. Nguyen, H. He, and C. Pham-Huy, "Chiral Drugs: An Overview," *International Journal of Biomedical Sciences* 2, no. 2 (2006): 85–100.

15. L. Weirich, G. Tusha, E. Engelage, L. V. Schäfer, and C. Merten, "VCD Spectroscopy Reveals Conformational Changes of Chiral Crown Ethers Upon Complexation of Potassium and Ammonium Cations," *Physical Chemistry Chemical Physics* 24, no. 19 (2022): 11721–11728.

16. K. Le Barbu-Debus, A. Scherrer, A. Bouchet, D. Sebastiani, R. Vuilleumier, and A. Zehnacker, "Effect of Puckering Motion and Hydrogen Bond Formation on the Vibrational Circular Dichroism Spectrum of a Flexible Molecule: The Case of (S)-1-Indanol," *Physical Chemistry Chemical Physics* 20, no. 21 (2018): 14635–14646.

17. A. Sklenář, L. Růžičková, V. Schrenková, et al., "Solid-State Vibrational Circular Dichroism for Pharmaceutical Applications: Polymorphs and Cocrystal of Sofosbuvir," *Spectrochimica Acta. Part A, Molecular and Biomolecular Spectroscopy* 318 (2024): 124478.

18. J. Frelek, M. Gorecki, M. Laszcz, A. Suszczynska, E. Vass, and W. J. Szczepek, "Distinguishing Between Polymorphic Forms of Linezolid by Solid-Phase Electronic and Vibrational Circular Dichroism," *Chemical Communications* 48, no. 43 (2012): 5295–5297.

19. M. Krupová, P. Leszczenko, E. Sierka, E. S. Hamplová, R. Pelc, and V. Andrushchenko, "Vibrational Circular Dichroism Unravels Supramolecular Chirality and Hydration Polymorphism of Nucleoside Crystals," *Chemistry - A European Journal* 28, no. 63 (2022): e202201922.

20. J. E. Rode, J. Wasilczenko, and M. Górecki, "Differentiation of Solvatomorphs of Active Pharmaceutical Ingredients (API) by Solid-State Vibrational Circular Dichroism (VCD)," *Spectrochimica Acta. Part A, Molecular and Biomolecular Spectroscopy* 310 (2024): 123851.

21. J. E. Rode, K. Łyczko, D. Kaczorek, R. Kawęcki, and J. Dobrowolski, "VCD Spectra of Chiral Naphthalene-1-Carboxamides in the Solid-State," *Spectrochimica Acta. Part A, Molecular and Biomolecular Spectroscopy* 310 (2024): 123939.

22. A. Scherrer, R. Vuilleumier, and D. Sebastiani, "Nuclear Velocity Perturbation Theory of Vibrational Circular Dichroism," *Journal of Chemical Theory and Computation* 9, no. 12 (2013): 5305–5312.

23. E. Ditler, T. Zimmermann, C. Kumar, and S. Luber, "Implementation of Nuclear Velocity Perturbation and Magnetic Field Perturbation Theory in CP2K and Their Application to Vibrational Circular Dichroism," *Journal of Chemical Theory and Computation* 18, no. 4 (2022): 2448–2461.

24. J. Blasius and B. Kirchner, "Selective Chirality Transfer to the Bis (Trifluoromethylsulfonyl)imide Anion of an Ionic Liquid," *Chemistry - A European Journal* 29, no. 51 (2023): e202301239.

25. S. Jähnigen, A. Zehnacker, and R. Vuilleumier, "Computation of Solid-State Vibrational Circular Dichroism in the Periodic Gauge," *Journal of Physical Chemistry Letters* 12, no. 30 (2021): 7213–7220.

26. M. M. Quesada-Moreno, A. Virgili, E. Monteagudo, et al., "A Vibrational Circular Dichroism (VCD) Methodology for the Measurement of Enantiomeric Excess in Chiral Compounds in the Solid Phase and for the Complementary Use of NMR and VCD Techniques in Solution: The Camphor Case," *Analyst* 143, no. 6 (2018): 1406–1416.

27. V. Declerck, A. Perez-Mellor, R. Guillot, D. J. Aitken, M. Mons, and A. Zehnacker, "Vibrational Circular Dichroism as a Probe of Solid-State Organisation of Derivatives of Cyclic Beta-Amino Acids: Cis- and Trans-2-Aminocyclobutane-1-Carboxylic Acid," *Chirality* 31, no. 8 (2019): 547–560.

28. J. R. Cheeseman, M. J. Frisch, F. J. Devlin, and P. J. Stephens, "Ab Initio Calculation of Atomic Axial Tensors and Vibrational Rotational Strengths Using Density Functional Theory," *Chemical Physics Letters* 252 (1996): 211–220.

29. P. Michal, J. Kapitán, J. Kessler, and P. Bouř, "Low-Frequency Raman Optical Activity Provides Insight Into the Structure of Chiral Liquids," *Physical Chemistry Chemical Physics* 24, no. 33 (2022): 19722–19733.

30. P. Bouř, J. Sopková, L. Bednárová, P. Maloň, and T. A. Keiderling, "Transfer of Molecular Property Tensors in Cartesian Coordinates: A New Algorithm for Simulation of Vibrational Spectra," *Journal of Computational Chemistry* 18 (1997): 646–659.

31. S. Yamamoto, X. Li, K. Ruud, and P. Bouř, "Transferability of Various Molecular Property Tensors in Vibrational Spectroscopy," *Journal of Chemical Theory and Computation* 8, no. 3 (2012): 977–985.

32. J. Kessler, J. Kapitán, and P. Bouř, "First-Principles Predictions of Vibrational Raman Optical Activity of Globular Proteins," *Journal of Physical Chemistry Letters* 6, no. 16 (2015): 3314–3319.

33. J. Kessler, T. A. Keiderling, and P. Bouř, "Arrangement of Fibril Side Chains Studied by Molecular Dynamics and Simulated Infrared and Vibrational Circular Dichroism Spectra," *Journal of Physical Chemistry B* 118 (2014): 6937–6945.

34. M. M. Quesada-Moreno, J. R. Avilés-Moreno, J. J. López-González, et al., "The Synergy of Different Solid-State Techniques to Elucidate the Supramolecular Assembly of Two 1H-Benzotriazole Polymorphs," *Physical Chemistry Chemical Physics* 21, no. 36 (2019): 19879–19889.

35. M. M. Quesada-Moreno, A. J. Cruz-Cabeza, J. R. Avilés-Moreno, et al., "The Curious Case of 2-Propyl-1H-Benzimidazole in the Solid State: An Experimental and Theoretical Study," *Journal of Physical Chemistry A* 121, no. 30 (2017): 5665–5674.

36. P. Ying, J. Yu, and W. Su, "Liquid-Assisted Grinding Mechanochemistry in the Synthesis of Pharmaceuticals," *Advanced Synthesis and Catalysis* 363, no. 5 (2021): 1246–1271.

37. S. Latif, Q. A. Ijaz, M. Hameed, et al., "Improvement of Physico-Mechanical and Pharmacokinetic Attributes of Naproxen by Co-crystallization with l-Alanine," *Journal of Drug Delivery Science and Technology* 61 (2021): 102236.

38. N. Tumanova, N. Tumanov, K. Robeyns, Y. Filinchuk, J. Wouters, and T. Leyssens, "Structural Insight into Cocrystallization with Zwitterionic Co-formers: Cocrystals of S-Naproxen," *CrystEngComm* 16, no. 35 (2014): 8185–8196.

39. T. Buffeteau, F. Lagugné-Labarthet, and C. Sourisseau, "Vibrational Circular Dichroism in General Anisotropic Thin Solid Films: Measurement and Theoretical Approach," *Applied Spectroscopy* 59, no. 6 (2005): 732–745.

40. C. Merten, T. Kowalik, and A. Hartwig, "Vibrational Circular Dichroism Spectroscopy of Solid Polymer Films: Effects of Sample Orientation," *Applied Spectroscopy* 62, no. 8 (2008): 901–905.

41. P. Bouř and T. A. Keiderling, "Partial Optimization of Molecular Geometry in Normal Coordinates and Use as a Tool for Simulation of Vibrational Spectra," *Journal of Chemical Physics* 117 (2002): 4126–4132.

42. J. Hudecová, K. H. Hopmann, and P. Bouř, "Correction of Vibrational Broadening in Molecular Dynamics Clusters with the Normal Mode Optimization Method," *Journal of Physical Chemistry B* 116 (2012): 336–342.

43. A. D. Becke, "Density-Functional Thermochemistry. III. The Role of Exact Exchange," *Journal of Chemical Physics* 98 (1993): 5648–5652.

44. M. J. Frisch, J. A. Pople, and J. S. Binkley, "Self-Consistent Molecular Orbital Methods 25. Supplementary Functions for Gaussian Basis Sets," *Journal of Chemical Physics* 80, no. 7 (1984): 3265–3269.

45. S. Grimme, S. Ehrlich, and L. Goerigk, "Effect of the Damping Function in Dispersion Corrected Density Functional Theory," *Journal of Computational Chemistry* 32, no. 7 (2011): 1456–1465.

46. M. J. Frisch, G. W. Trucks, H. B. Schlegel, et al., *Gaussian 16 rev. a.03* (Wallingford, CT: Gaussian, Inc, 2016).

47. J. Kapitán, V. Baumruk, V. Kopecký, Jr., R. Pohl, and P. Bouř, "Proline Zwitterion Dynamics in Solution, Glass and Crystalline State," *Journal of the American Chemical Society* 128, no. 41 (2006): 13451–13462.

48. A. Klamt, "COSMO and COSMO-RS," in *The Encyclopedia of Computational Chemistry*, vol. 1, eds. P. R. Schleyer, N. L. Allinger, T. Clark, et al. (Chichester: John Wiley & Sons, 1998): 604–615.

49. M. Born and K. Huang, *Dynamical Theory of Crystal Lattices* (Oxford: Oxford Academic, 1996).

50. A. Tilborg, G. Springuel, B. Norberg, J. Wouters, and T. Leyssens, "On the Influence of Using a Zwitterionic Coformer for Cocrystallization: Structural Focus on Naproxen–Proline Cocrystals," *CrystEngComm* 15, no. 17 (2013): 3341–3350.

51. J. Kubelka, J. Kim, P. Bouř, and T. A. Keiderling, "Contribution of Transition Dipole Coupling to Amide Coupling in IR Spectra of Peptide Secondary Structures," *Vibrational Spectroscopy* 42, no. 1 (2006): 63–73.

52. J. Kessler, V. Andrushchenko, J. Kapitán, and P. Bouř, "Insight into Vibrational Circular Dichroism of Proteins by Density Functional Modeling," *Physical Chemistry Chemical Physics* 20, no. 7 (2018): 4926–4935.

53. H. Sato and I. Kawamura, "Solid-State Vibrational Circular Dichroism Studies on the Conformation of an Amino Acid Molecule in Crystalline State," *Biochimica et Biophysica Acta, Proteins and Proteomics* 1868 (2020): 140439.

54. S. Jähnigen, "Vibrational Circular Dichroism Spectroscopy of Chiral Molecular Crystals: Insights from Theory," *Angewandte Chemie, International Edition* 62, no. 41 (2023): e202303595.

55. S. Jähnigen, K. Le Barbu-Debus, R. Guillot, R. Vuilleumier, and A. Zehnacker, "How Crystal Symmetry Dictates Non-local Vibrational Circular Dichroism in the Solid State," *Angewandte Chemie, International Edition* 62, no. 5 (2023): e202215599.

56. S. Jähnigen, A. Scherrer, R. Vuilleumier, and D. Sebastiani, "Chiral Crystal Packing Induces Enhancement of Vibrational Circular Dichroism," *Angewandte Chemie, International Edition* 57, no. 40 (2018): 13344–13348.

57. K. Le Barbu-Debus, J. Bowles, S. Jähnigen, et al., "Assessing Cluster Models of Solvation for the Description of Vibrational Circular Dichroism Spectra: Synergy Between Static and Dynamic Approaches," *Physical Chemistry Chemical Physics* 22, no. 45 (2020): 26047–26068.

Supporting Information

Additional supporting information can be found online in the Supporting Information section.